Hollow CeO2 Nanospheres as Catalyst for the Conversion of Aromatic Diamines to Benzimidazoles

Journal:	*ACS Applied Nano Materials*
Manuscript ID	an-2023-05323j.R2
Manuscript Type:	Article
Date Submitted by the Author:	n/a
Complete List of Authors:	Srinivasappa, Puneethkumar; Jain University, Centre for Nano and Material Sciences Singh, Chob; JAIN (Deemed-to-be-university) Centre for Nano and Material Sciences Alla, Sarat; JAIN (Deemed-to-be-university) Centre for Nano and Material Sciences Gholap, Sandeep; King Abdullah University of Science and Technology Physical Sciences and Engineering Division, INSTITUTE OF SUSTAINABILITY FOR CHEMICALS, ENERGY AND ENVIRONMENT (ISCE²) Samal, Akshaya K; Jain University - Ramanagara Campus, Centre for Nano and Material Sciences Chaudhari, Nitin; Pandit Deendayal Petroleum University, Department of Chemistry Jadhav, Arvind; Jain University, Centre for Nano and Material Sciences

Hollow CeO_2 Nanospheres as Catalyst for the Conversion of Aromatic Diamines to Benzimidazoles

Puneethkumar M. Srinivasappa,[a] Chob Singh,[a] Sarat Chandra Alla,[a] Sandeep Suryabhan Gholap,[b] Akshaya K. Samal,[a] Nitin K. Chaudhari,[c] Arvind H. Jadhav*,[a]

[a]*Centre for Nano and Material Science, Jain University, Jain Global Campus, Bangalore 562112, Karnataka, India.*

[b]*Catalysis and Green Process Engineering, Institute of Sustainability for Chemicals, Energy and Environment, 1 Pesek Road, Jurong Island, Singapore-627833*

[c]*Advanced Hybrid Nanomaterial Laboratory, Department of Chemistry, School of Energy Technology, Pandit Deendayal Energy University, Gandhinagar, 382426, Gujarat, India*

Corresponding Author:* ***j.arvind@jainuniversity.ac.in; jadhav.ah@gmail.com*

GRAPHICAL ABSTRACT

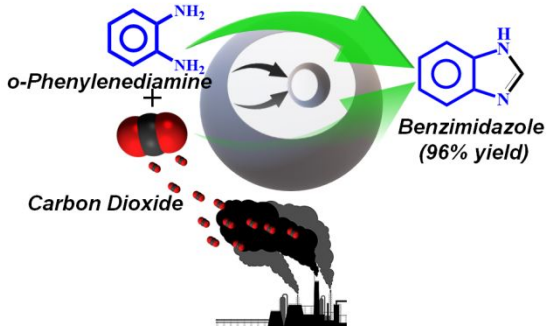

ABSTRACT: Utilization of anthropogenic CO_2 towards valuable heterocyclic compounds is a very significant strategy to alleviate environmental issues. Herein, solvothermal method-assisted synthesized hollow CeO_2 nanospheres (HNS-CeO_2) material was employed as an efficient catalyst for the selective benzimidazole synthesis under neat and temperate reaction conditions. Examined controlled reaction conditions for the design of HNS-CeO_2 material through the study of various reaction parameters. Very interestingly, the HNS-CeO_2 material observed different surface morphology disparities from the effect of various reaction

parameter studies that were examined by using FE-SEM analysis comprehensively. Systematically well characterized the HNS-CeO_2 material by using various analytical and spectroscopic techniques. The competent catalyst of HNS-CeO_2 showed superior catalytic activity (100% conversion, 96% selectivity, and yield) under mild reaction conditions and these conditions are successfully identified by studying the effect of various reaction parameters. Remarkably, the inherent properties of the HNS-CeO_2 catalyst boosted the synergistic effect with the model reagents of DMAB, and base. Moreover, different functional groups substituted benzimidazole compounds are successfully synthesized in good to excellent yields under optimized reaction conditions. The effective contribution of DMAB, base, Lewis acidic, and Lewis basic sites were successfully revealed by proposing a tentative benzimidazole reaction mechanism. Notably, the examined 15 successive recycles with stable catalytic activity performance demonstrated the stable catalytic activity, structural and physicochemical properties of the HNS-CeO_2 catalyst.

KEYWORDS: *CO_2 fixation; hollow CeO_2 nanospheres; cycloaddition reaction; benzimidazole; synergistic benzimidazole mechanism*

1. INTRODUCTION

Metal or mixed metal oxides are widely used as promising materials in novel fields of chemistry such as thermo/photo/electrocatalysis, sensing, biological chemistry, water splitting, environmental remediation, solar cells, polishing materials, batteries, and so on.[1, 2] Amongst them, the earth-abundant elemental oxide of CeO_2 was extensively explored in eminent fields due to its physicochemical properties like thermal and chemical stability, acidic and basic sites, redox properties, abundant oxygen vacancies, and oxygen storage capacity.[3, 4] Therefore, the CeO_2 has been extensively explored as an efficient catalyst for

various organic transformations.[5] Interestingly, based on earlier reports, inherent properties of the CeO_2 are highly reliant on surface morphology and synthesis approach. Earlier reports are well explored CeO_2 catalyst different surface morphologies (porous, spheres, cubic, star, rods, wires, and hollow spheres) along with excellent inherent properties with the assistance of various synthesis methods.[1, 6, 7] Nowadays, a few research groups were synthesized hollow CeO_2 spheres using various capping agents via various approaches.[8-11] Recently, significant efforts have been devoted to the synthesis of hollow CeO_2 spheres under facile, capping agent-free, and mild reaction conditions. Hence, it is very challenging and has attracted great interest in material design. So, a systematic approach for the synthesis of hollow CeO_2 spheres material has not been explored to date. Very attractively, hollow nanospheres structural morphology extensively endorses the material physicochemical properties such as crystallinity, porosity, specific surface area, diffusion of reagents, and exposure of active sites on its surface.[11, 12] To the best of our knowledge, the design of hollow CeO_2 nanospheres that could be used as a thermocatalyst is highly favorable for organic transformations.

Recently, among various organic transformations, the carbon dioxide (CO_2) fixation protocols have become one of the most attractive strategies in scientific research filed. The uncontrollable emission of CO_2 from burning of fossil fuels, rapid industrial evolution, deforestation, gasoline vehicles, and so on.[13, 14] Subsequently, due to these issues, the concentration of greenhouse gases are gradually increasing and it has been reached 419 ppm in the atmosphere.[15] Among greenhouse gases, CO_2 has been identified as the primary culprit in the environment. Hence, emerging innovative tactics to lessen anthropogenic CO_2 concentration through synthesis of value-added chemicals is an impressive task in the research field.[16, 17] Using CO_2 as the C1 source, earlier were synthesized the various value-added chemicals, namely methanol, formic acid, hydrocarbons, heterocyclic compounds, and so on.[17, 18] Heterocyclic compounds are broadly applicable in pharmaceuticals,

agrochemicals, drug design, as solvents, reagents, Li-ion batteries, and more.[19] Thus, the design of novel thermocatalysis for the benzimidazole synthesis via the fixing of CO_2 is great catalytic efficiency at the industrial level. Previously, only a few efficient homogeneous and heterogeneous catalysts were reported for the benzimidazole synthesis.[20-22] However, earlier reported catalysts required harsh reaction conditions and solvents to enhance the catalytic activity. So, the development of an efficient thermocatalyst with the selective features of a non-nobel, highly recyclable, stable, and highly active catalyst under green reaction conditions is a very great challenge for the CO_2 fixation reaction.

Herein, the development of pioneering research ideas towards lessening of CO_2 concentration via fixation of CO_2 into the heterocyclic compound of benzimidazole is a very attractive strategy. In our investigation, hollow CeO_2 nanospheres (HNS-CeO_2) material was successfully synthesized by using a solvothermal method under controlled reaction conditions. The controlled reaction conditions are succinctly optimized by examining various reaction parameters such as effect of temperature, time, solvent, solvent ratio, calcination temperature, and time. The observed different surface morphology disparities of the HNS-CeO_2 material were examined by using FE-SEM analysis. With the support of FE-SEM analysis results, revealed the Ostwald ripening process was significantly contributed to the formation of hollow CeO_2 nanospheres. Moreover, the inherent properties of the HNS-CeO_2 material were examined using various analytical and spectroscopic techniques such as thermogravimetric analysis (TGA), X-ray diffraction (XRD), high-resolution transmission electron microscopy (HR-TEM), Fourier transformation infrared spectroscopy (FT-IR), Raman, pyridine adsorption, chloroform adsorption and X-ray photo-electron spectroscopy (XPS), analysis. All results are taken into consideration, the HNS-CeO_2 material tested as an efficient catalyst for the cycloaddition reaction between CO_2 and o-phenylenediamine. The HNS-CeO_2 catalyst showed superior catalytic activity with 100% conversion of OPD and

96% yield, along with selectivity of the benzimidazole product under temperate reaction conditions. The temperate reaction conditions were scrutinized by examining effect of various reaction parameters such as effect of base, DMAB, catalyst amount, temperature, pressure, and time. Moreover, synthesized various functional groups anchored benzimidazole compounds under optimized reaction conditions and achieved moderate to excellent yields of the desired product using promising catalyst of HNS-CeO_2. Also, evidently revealed the effective active sites (Lewis acidic and Lewis basic) synergistic effect, role of DMAB, and base in the proposed plausible benzimidazole reaction mechanism. Remarkably, the stable recyclability feature of the HNS-CeO_2 catalyst (for up to 15 consecutive cycles) gives the great potential application for the CO_2 fixation reaction. Evidently demonstrated the spent catalyst stable structural and physicochemical properties with the help of XRD, FE-SEM, EDAX, mapping, TEM/HR-TEM and XPS analysis. Hence, the existing ideal procedure is highly favorable to the selective synthesis of a value-added product under mild, clean and green reaction conditions.

2. RESULTS AND DISCUSSION

2.1 Examination of HNS-CeO_2 Material Inherent Properties by Using Various Analytical and Spectroscopic Techniques

Successfully synthesized the HNS-CeO_2 material via a solvothermal method **(Scheme S1)**. When compared to earlier reports, the established procedure for the HNS-CeO_2 material is most prominent and cost-effective because, it is capping agent-free, a shorter reaction time, a lower reaction temperature, and used greener solvents, namely 1-propanol and glycerol. After successful synthesis of the HNS-CeO_2, initially we examined the thermal stability and crystallinity of the synthesized materials.

Initially, we scrutinized the thermal stability of the HNS-CeO_2 material using TGA analysis and obtained thermogram as depicted in **Figure 1 (a)**. As per earlier reports, a chosen annealed temperature is enough to convert the hydroxide phase (NS-$Ce(OH)_3$) into the oxide phase (HNS-CeO_2). As displayed in **Figure 1 (a)**, the TGA thermogram clearly detects two decomposition steps at RT-135 °C and 136-387 °C. The initial weight loss of 1.28% is attributed to the physically adsorbed surface hydroxide groups on the material surface. The second-step weight loss value of 2.11% is due to the decomposition of residual solvents used in the synthesis procedure.[23] Finally, in higher temperature region (>400 °C), the HNS-CeO_2 material did not observe any decomposition step. Hence, we are strongly concluded that the synthesized HNS-CeO_2 material has high thermal stability and can be effectively used as an efficient thermocatalyst for CO_2 fixation reactions.

Next, we inspected the crystallographic structure and phase purity of NS-$Ce(OH)_3$ and HNS-CeO_2 materials using XRD analysis **(Figure 1 (b))**. The XRD profile of the uncalcined NS-$Ce(OH)_3$ material observed broad peaks at different 2 theta positions (28.85, 47.64, and 56.45°), which indicates the synthesized material is an amorphous in nature. The NS-$Ce(OH)_3$ material peaks are wider due to the erection of smaller crystals and the presence of hydroxide functional groups. According to the TGA analysis results, after a calcination process, there was no any detectable decomposition step in the HNS-CeO_2 material **(Figure 1 (a))**. The HNS-CeO_2 material XRD pattern achieved well-established distinctive peaks at different 2 theta positions 28.55, 33.07, 47.48, 56.34, 59.09, 69.35, 76.76, and 79.08°. All distinctive peaks are well credited to the (111), (200), (220), (311), (222), (400), (331), and (420) planes of the cubic fluorite HNS-CeO_2 structure (JCPDS no. 34-0394).[21, 24] Evidently, the observed HNS-CeO_2 material XRD pattern indicates that high crystallinity and purity without observing any impurities. Additionally, crystallite sizes were calculated by using

Debye-Scherrer formula (D=(0.89xλ)/(βxcosθ)), and both NS-$Ce(OH)_3$ and HNS-CeO_2 materials are associatively achieved crystallite sizes of 1.75 nm and 10.24 nm.[4] The achieved crystalline (111) plane in the synthesized HNS-CeO_2 material might be enhances active surface area. After the calcination process, the broad peaks of the hydroxide material are well converted into sharp peaks, which strongly indicates the enhancement of crystallinity in the HNS-CeO_2 material.

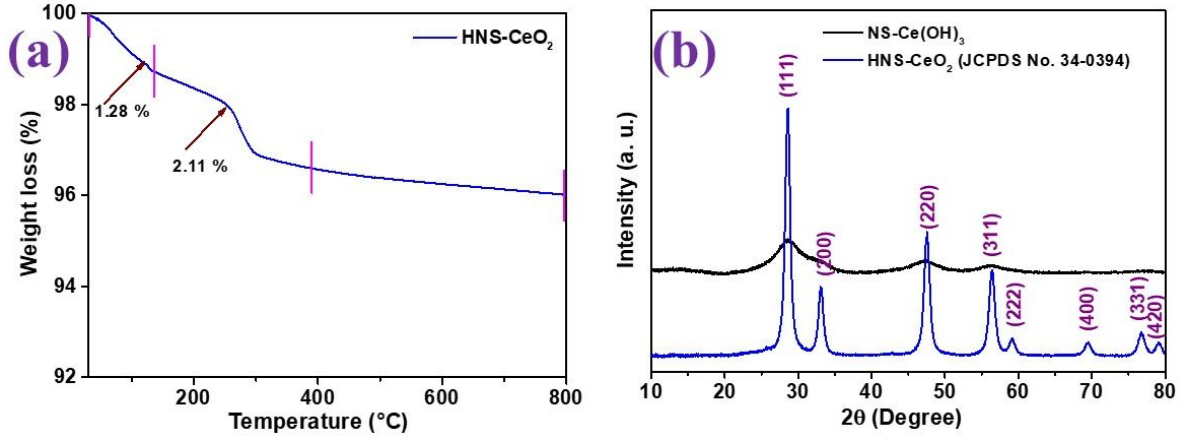

Figure 1. TGA analysis of HNS-CeO_2 **(a)** and XRD analysis of NS-$Ce(OH)_3$ and HNS-CeO_2 **(b)** materials.

Later, we examined the surface architecture of both NS-$Ce(OH)_3$ and HNS-CeO_2 materials using FE-SEM analysis and depicted all images in **Figure 2 (a–i).** The NS-$Ce(OH)_3$ material surface morphology images are displayed in **Figure 2 (a–c).** The NS-$Ce(OH)_3$ material surface successfully observed nanospheres. After the calcination process the HNS-CeO_2 material evidently exhibited hollow nanospheres morphology, as shown in **Figure 2 (d-i)**. At lower magnification levels, image **d** displays spheres morphology with hollow nature. Further increasing the magnification, the HNS-CeO_2 material surface clearly exhibited a clear hollow nature (images **e** and **f)**. Images **g, h,** and **i** evidently indicates an individual nanosphere with a hollow nature, and these spheres evidently observed excellent hollow pore diameter. The hollow nanospheres morphology effectively boosts their thermal stability,

crystallinity, specific surface area, effective active site concentration, and easy availability of active sites on its surface.[25]

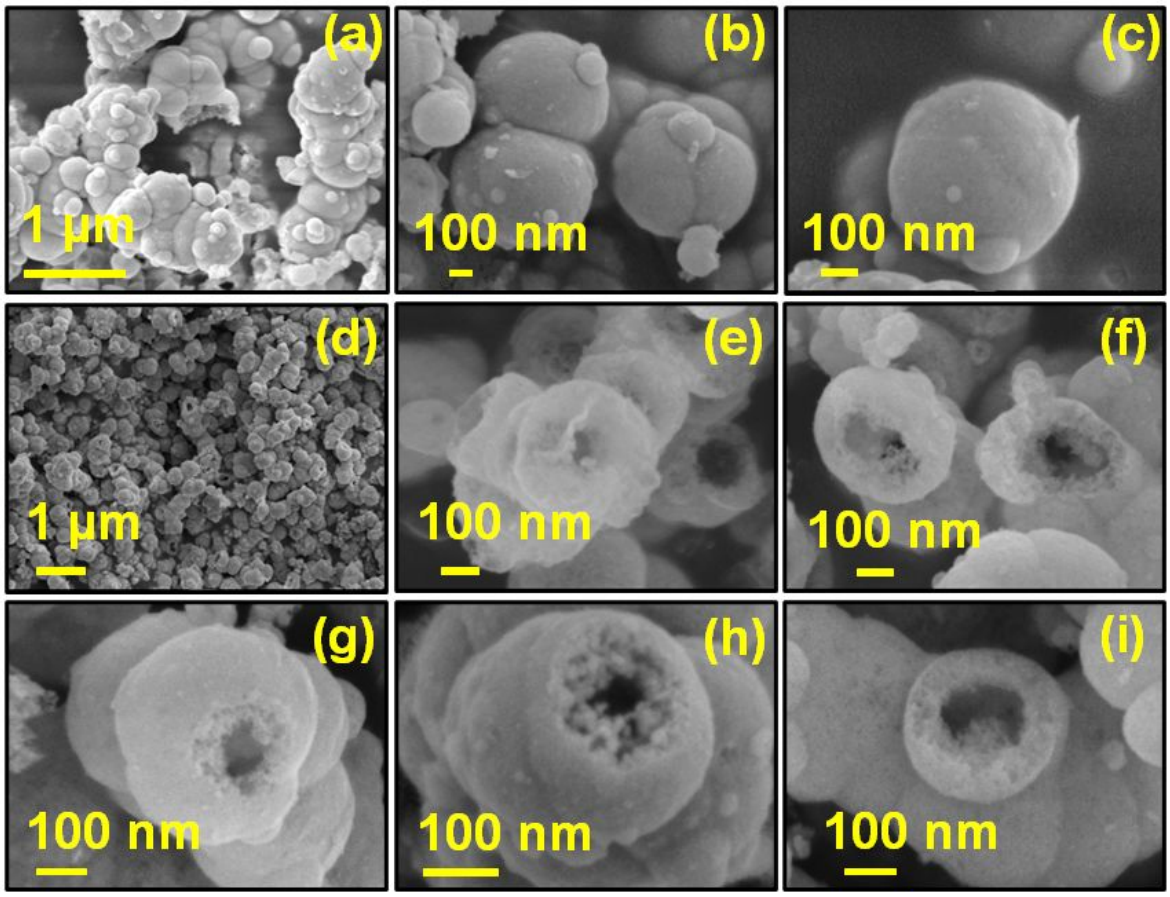

Figure 2. FE-SEM analysis images of NS-$Ce(OH)_3$ **(a-c)** and HNS-CeO_2 **(d-i)**.

Further evidently confirmed the hollow nanospheres morphology of the HNS-CeO_2 material by examining TEM and HR-TEM analysis, the obtained analysis images are shown in **Figure 3**. The initial three images **(Figure 3 (a, b, c))** signify the low and high magnification TEM analysis results. **Figure 3 (a)** evidently concluded that the formation of uniform hollow nanospheres morphology, and these results are well in accordance with the observed FE-SEM analysis results **(Figure 2 (d-i))**. The images **b** and **c** clearly observed the strong contrast between the intensely shady margins and the light pale region in the center, which gives resilient proof for the existence of hollow nanospheres morphology of the HNS-

CeO_2 material.[8] **Figure 3 (d and e)** images indicated the HR-TEM analysis results in that the image **d** clearly indicate the hollow nanospheres are self-possessed by the number of interconnected smaller CeO_2 nanoparticles.[10] Using image **e**, the calculated lattice spacing value of 0.29 nm is well corresponds with the (220) plane of the highly crystalline HNS-CeO_2 material. The displayed SAED (selected-area electron diffraction) pattern image **f**, the concentric circles along with the mentioned (hkl) values indicates that the polycrystalline nature and a cubic fluorite phase of the synthesized HNS-CeO_2 material.[26]

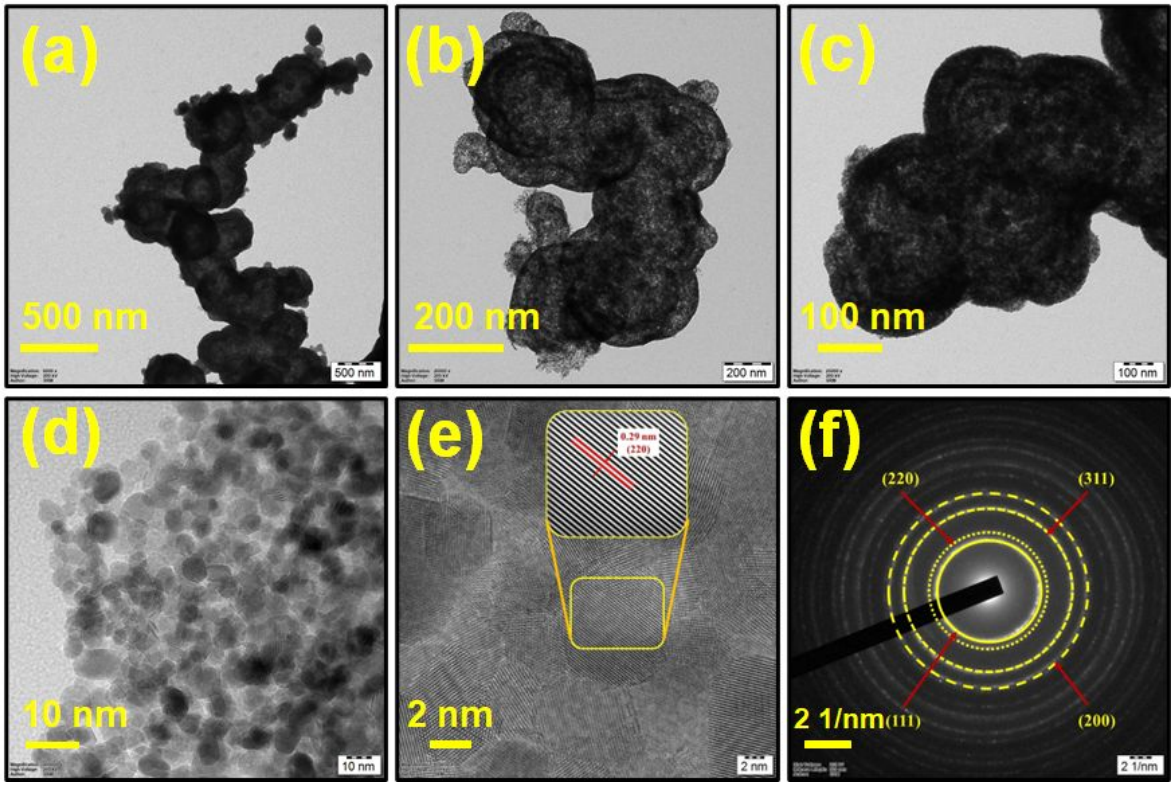

Figure 3. TEM **(a-c)**, HR-TEM **(d and e)** and SAED pattern **(f)** analysis of HNS-CeO_2.

In this work, solvothermal method was assisted for the design of HNS-CeO_2 material using a 35:15 mL solvent ratio (propanol: glycerol), 190 °C for 5 h (10 °C/min), and annealed at 500 °C for 6 h (10 °C/min). The HNS-CeO_2 material surface morphology was confirmed by using FE-SEM analysis **(Figure 2 (d-i))**. More evidently, the hollow nanospheres architecture was confirmed by using TEM and HR-TEM analysis **(Figure 3 (a-f))**.

Additionally, we inspected the effect of reaction temperature, reaction time, solvent, solvent ratio, calcination temperature, and time for the hollow nanospheres formation process. Very interestingly, examined the observed different surface morphology disparities from the effects of various parameters by using FE-SEM analysis. Also, evidently found the intensive key roles of glycerol and propanol solvents in the hollow nanosphere's formation process.

Effect of Solvothermal Reaction Temperature. In a solvothermal method, the reaction temperature plays a very critical role to design the hollow nanospheres morphology.[27] Initially, we examined the effect of reaction temperature in the region of 170 to 200 °C, and rest of the reaction conditions were kept constant (solvent ratio, reaction time, calcination temperature and time). **Figure S1** depicts the observed surface morphology images for all samples. The suitable reaction temperature effectively enhances the nucleation and particle growth towards the expected hollow nanospheres morphology. Initially, the tested 170 °C reaction temperature product surface evidently observed clear nanospheres morphology **(Figure S1 (a, b))**. **Figure S1 (c)** image evidently depicts that inner crystallites are started to decompose via the Ostwald ripening process to get the hollow morphology.[8] The 180 °C reaction temperature sample surface results are observed to have a nanospheres morphology with a hollow nature, as shown in **Figure S1 (d and e)**. **Figure S1 (f)** image clearly indicates that hollow nanosphere morphology was observed with a smaller hollow pore diameter when compared to **Figure 2 (e)**. When compared to the 170 °C, the 180 °C material surface was observed larger hollow pore diameter due to the decomposition of inner crystallites in side nanospheres. Further increasing the reaction temperature up to 200 °C, the hollow nanospheres morphology was started to destroy, as displayed in **Figure S1 (g, h)**. Also, hollow nanospheres are observed more roughness and decreased the thickness of the nanosphere, as shown in **Figure S1 (i)**. Therefore, a reaction temperature of 190 °C is highly

suitable to form a well hollow pore diameter with a greater thickness of the nanospheres for the synthesis of HNS-CeO_2 material.

Effect of Solvothermal Reaction Time. To notice hollow nanospheres morphology growth, time-dependent reactions are carried out under the optimized reaction temperature at 190 °C, and remaining reaction conditions are kept constant (solvent ratio, calcination temperature, and time). With increasing the reaction time, we observed the formation of appropriate hollow nanospheres with excellent hollow pore diameter and thickness of the shell. When examine the surface morphology of the 3 h product surface, only nanospheres morphology was observed **(Figure S2 (a–c)),** along with achieved lower HNS-CeO_2 product yield. Further prolonged the reaction time up to 4 h, the surface morphology exhibits a hollow with a nanospheres like morphology. But, when the surface is magnified, **Figure S2 (f)** image clearly indicates that decomposition of inner crystallites is under progress. Further, examined the extended reaction time product (5 h) and clearly observed excellent hollow pore diameter and thickness of the hollow nanospheres, as shown in **Figure 2 (e-i)**. However, beyond 5 h reaction time product surface morphology was decomposed due to the expense of nuclei growth in the reaction medium, as shown in **Figure S2 (g-i)**. Hence, the 5 h reaction time is ideal reaction time to achieve excellent nuclei growth with high yield, and to get clear hollow nanospheres morphology of the HNS-CeO_2 product at 190 °C.

Effect of Solvent and Solvent Ratio. In the solvothermal method, the solvent/solvents and solvent ratio play a very significant role in governing specific morphology.[28] With the aid of earlier reports, propanol and glycerol were chosen as suitable green solvents for the synthesis of hollow CeO_2 nanospheres. Initially, we synthesized the CeO_2 product by using 50 mL of individual solvents of propanol and glycerol under optimized reaction conditions of 190 °C for 5 h, and other reaction conditions were kept constant (calcination temperature and time). The propanol solvent product surface successfully observed uniform nanospheres

morphology **(Figure S3 (a–c))**. But the glycerol solvent failed to achieve the NS-$Ce(OH)_3$ product under considered solvothermal reaction conditions. It was strongly suggested that the propanol solvent directly helps to the soluble of Ce precursor in the reaction medium for redox reactions, nucleation, self-aggregation, and hydrogen bonding with the glycerol reagent. It was successfully confirmed that both solvents are more important to the design of hollow nanospheres. Further, we scrutinized the optimal solvent ratio for the synthesis of HNS-CeO_2 by studying the effect of solvent ratio. The solvent ratio was started with a ratio of 25:25 (glycerol: propanol). As shown in **Figure S4 (a–c)**, all images are clearly demonstrated that the agglomeration of particles on the surface without detecting any specific surface morphology. Further by decreasing the glycerol amount, we tested the 20:30 (glycerol: propanol) solvent ratio reaction. As evidently displayed in **Figure S4 (d–f)**, the surface was observed spheres along with rods morphology. When the surface is magnified, observe the decomposition of hollow nanosphere morphology, as shown in **Figure S4 (f)**. Further, we decreased the glycerol amount and tested the 15:35 mL (glycerol: propanol) solvent ratio and obtained surface morphology images are attested in **Figure 2 (d–i).** It is evidently observed that the clear hollow nanospheres morphology without observing any debris on its surface. The obtained hollow nanospheres morphology was successfully observed to have excellent hollow pore diameter and thickness of the shell. When further decreased the glycerol ratio to 10:40 (glycerol: propanol), the observed results **(Figure S4 (g-i))** evidently revealed that the 15:35 (glycerol: propanol) ratio is highly appropriate and an optimized solvent ratio for the synthesis of the HNS-CeO_2 product. It is remarkably noticed that the 15:35 mL solvent ratio medium tremendously controlled the nucleation speed, faster crystallite growth, and higher crystallinity under optimized reaction conditions at 190 °C for 5 h. The effects of the solvents, propanol and glycerol ratios, evidently proved that glycerol is

a highly desirable solvent to encourage hollow nanospheres morphology in the solvothermal method.

Effect of Calcination Temperature and Time. The structural stability and the formation of the hollow nanosphere's morphology is completely reliant on the calcination temperature and time. It is very noteworthy to examine the surface morphologies affected by calcination temperature and time products. As shown in **Figure S5 (a–b)**, initially the chosen 450 °C annealed temperature product surface was clearly observed nanospheres morphology. **Figure S5 (c)** clearly indicates that the decomposition of inner crystallites is started. Also, the obtained results are evidently indicating that high temperature is required to get excellent hollow nanospheres morphology. Further, 500 °C temperature product surface clearly achieved hollow nanospheres morphology, as shown in **Figure 2 (d-i)**. Later, increased the calcination temperature up to 600 °C. Both 550 °C **(Figure S5 (d-f))** and 600 °C **(Figure S5 (g-i))** products surface morphology evidently observed disintegration of hollow nanospheres. Additionally, crystallinity nature and crystallite sizes are correspondingly increased by increasing the calcination temperature, as shown in **Figure S6**. Later, scrutinized the effect of calcination time products (4, 5, 6, and 7 h) surface morphology **(Figure S7)**. The 4 h sample clearly observed nanospheres morphology without detecting hollow morphology, as shown in **Figure S7 (a–c)**. The time-extended sample (5 h) surface was observed hollow nanospheres **(Figure S7 (d-e))**. The magnified image **(Figure S7 (f))** clearly indicates that hollow nanospheres formation process is in progress via the Ostwald ripening method. Further, the extended calcination time (6 h) sample surface clearly observed hollow nanospheres with a high hollow pore diameter and thickness of the shell **(Figure 2 (d-i)).** Later, the extended calcination time (7 h) product surface clearly observed decomposition of hollow nanosphere morphology, as displayed in **Figure S7 (g-i)**.

Remarkably, from the FE-SEM analysis results evidently concluded the optimized solvothermal reaction conditions (190 °C, 5 h, 15:35 (glycerol: propanol) solvent ratio, and 500 °C for 6 h) for the design of excellent hollow CeO_2 nanospheres (HNS-CeO_2) material. Based on the FE-SEM analysis results, the HNS-CeO_2 material surface was chosen as a promising material to examine other analytical and spectroscopic techniques.

2.2 Schematic Possible Mechanism Strategy for Hollow CeO_2 Nanospheres

In the preceding section, a detailed study of effect of various reaction parameters are discussed in detail, and the formation of hollow nanosphere's mechanism was traced by using FE-SEM analysis. Earlier, several research groups rationally proposed the hollow nanospheres formation mechanism.[8, 29] In solvothermal processes, the ratio between propanol and glycerol, reaction time, reaction temperature, calcination temperature, and time will play a very decisive roles in the nucleation and stabilization of the $Ce(OH)_3$ steps. Based on the observed FE-SEM results, in solvothermal process unquestionably change the surface morphology if the reaction parameters were changed.

Based on observed results and with the aid of earlier reports, we proposed the schematic representation for the formation of hollow nanospheres mechanism, as shown in **Figure S8**. Unlike in the solvothermal process, hollow nanospheres morphology evolves specifically through a nucleation, self-assembly, and Ostwald ripening steps.[30] As mentioned in **Figure S8**, under solvothermal conditions, the cerium precursor easily undergoes a redox reaction with the help of propanol. Meanwhile, it produces the suspension solution with the precursor via strong intermolecular hydrogen bonding between glycerol and propanol. Hence, the faster nucleation rate under heating conditions helps to produce smaller crystallites in the reaction medium. By reducing the surface energy in the reaction medium and by a self-aggregation, numerous crystalline particles are successively promoted into larger particles as

a nanosphere. Higher-temperature reaction conditions are highly favorable to the initial steps of nucleation and aggregation, and these steps are completely reliant on the solvent ratio, reaction time, and reaction temperature. The constructed nanospheres with the assistance of nanoparticles, the inner crystallites are easily decomposed than the external crystallites via the Ostwald ripening process. When the hydroxide material of (NS-$Ce(OH)_3$) proceeds for annealing, it achieves a hollow nanosphere morphology through the successful decomposition of the interlayer glycerate precursor. As a result, the nanosphere successfully transformed into a hollow structure with better crystallinity and a well-swelled hollow spherical shape.[8, 25, 31, 32]

The functional groups of NS-$Ce(OH)_3$ and HNS-CeO_2 materials were studied by using FT-IR analysis, and obtained spectra are shown in **Figure S9 (a)**. The uncalcined material of Ce hydroxide surface detects multiple peaks at different wavelength regions. The broad peak at 3250–3700 cm^{-1} indicates the presence of stretching vibrations of OH groups due to the presence of glycerol and propanol functional groups. The peaks at 2926 and 1620 cm^{-1} belong to the stretching vibration functional groups of C-H and C=O, respectively. The additional peaks at 1390 and 1100 cm^{-1} correspond to the bending vibrations of C-H and the stretching vibration of C-N bond. The peaks at the 800-600 cm^{-1} region assigned for the NO_3^- groups are present in the cerium hydroxide material. The Ce-OH group peak at 470 cm^{-1} in the NS-$Ce(OH)_3$ spectrum.[25, 33] After, we clearly observed the metal oxygen stretching peak (Ce-O-Ce) at 518 cm^{-1} in the HNS-CeO_2 surface. The HNS-CeO_2 material observed M-O stretch peaks at 1086 and 1369 cm^{-1}. Also, the HNS-CeO_2 surface observed OH bending and stretching peaks at 1585 and 3397 cm^{-1} due to the presence of physically adsorbed moisture on the HNS-CeO_2 surface.[21, 34]

The HNS-CeO_2 material Raman spectrum as shown in **Figure S9 (b)**. The observed strong intense peak at 463 cm^{-1} belongs to the Ce-O vibration bond (symmetrical stretching), and it corresponds to the phase of fluorite F_{2g} mode. Interestingly, the HNS-CeO_2 material showed peak at 614 cm^{-1}, which demonstrates the defective D mode band of the intrinsic oxygen vacancies due to the presence of Ce^{3+} species in the HNS-CeO_2 material.[34, 35] To find the oxygen vacancies, integrated both areas of I_D and I_{F2g} peaks and achieve a value of 0.0780. The observed oxygen vacancies enhance the reduction properties of the HNS-CeO_2 material. Very interestingly, the oxygen vacancies act as Lewis acidic sites and effectively enhance CO_2 activation very easily in CO_2 fixation reactions.[36]

Examined the presented elements and distribution of elements in the synthesized HNS-CeO_2 material by using EDAX analysis and elemental mapping, respectively. As shown in **Figure S10 (a)**, the survey spectrum detects the presence of elements, namely, Ce and O in the HNS-CeO_2 material. Additionally, **Figure S10 (b-d)** images clearly indicate the uniform distribution of Ce and O elements in the HNS-CeO_2 material. The obtained EDAX and elemental mapping analysis results evidently revealed that without detecting any impurity elements, the HNS-CeO_2 material achieved a uniform distribution of active sites (Ce, O) on its surface.

The acidic (Lewis acidic) and basic (Lewis basic) type of sites have been previously examined by using pyridine and chloroform adsorption techniques with the help of FT-IR instrument. Successfully, we executed both techniques for the HNS-CeO_2 material. The engaged surface Lewis acidic sites (Ce cations) in the HNS-CeO_2 detect the peak at 1618 cm^{-1} **(Figure 4 (a))**. However, the observed peak at a higher wavenumber evidently indicates the strong Lewis acidic sites were occupied in the HNS-CeO_2. The less intense broad peak at

1552 cm^{-1} belongs to the Brønsted acidic sites that were occupied on the surface with less concentration. The broad peak at 1489 cm^{-1} belongs to the coordinatively bonded pyridine, or PyH^{+} (hydrogen-bonded pyridine), with the HNS-CeO_2 surface. Additionally, uncoordinated oxygen sites in the HNS-CeO_2 are executed by performing the chloroform adsorption analysis, as shown in **Figure 4 (b)**. The spectrum detects a broad peak with a hump at 2972 and 2913 cm^{-1}, which are ascribed to the $CHCl_3$ being interacted with uncoordinated oxygen sites (O^{2-}----$HCCl_3$) as an end-on mode. Additionally, due to the presence of Lewis acidic sites in the HNS-CeO_2, the Cl molecules will interact with the Lewis acidic sites, and we observed the merged peak at 2972 cm^{-1}. Hence, both pyridine and chloroform adsorption techniques are evidently revealed that the presence of Lewis acidic (Ce cations) and Lewis basic sites (Ce-O^{2-}) in the HNS-CeO_2 surface. Successfully occupied both Lewis acidic (Ce cations) and Lewis basic sites are highly influences the activity enhancement in the CO_2 fixation reactions.[24]

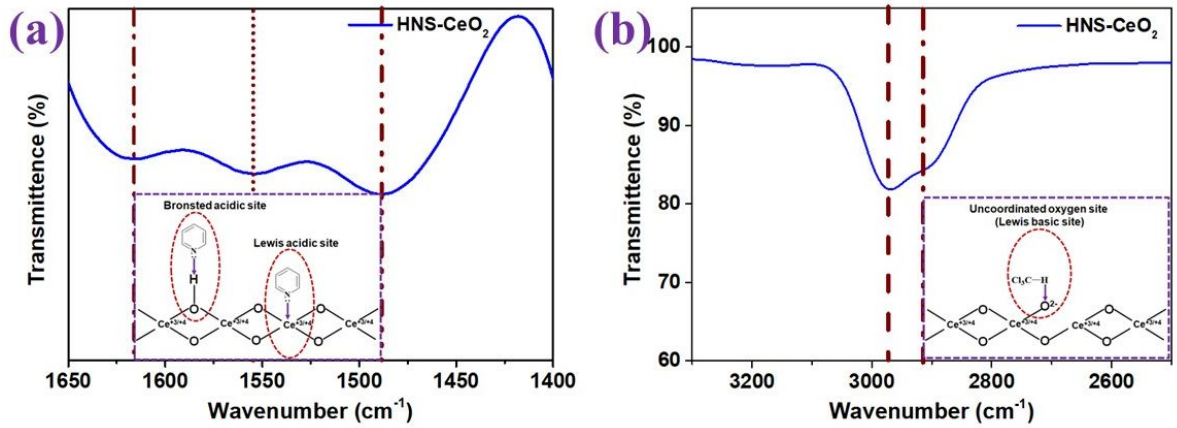

Figure 4. HNS-CeO_2 material pyridine adsorption **(a)** and chloroform adsorption **(b)** analysis.

2.3 Initial Catalyst Screening Study for Benzimidazole Synthesis Via CO_2 Fixation Process

Successfully explored ideal reaction conditions for the design of HNS-CeO_2 material along with hollow nanospheres formation mechanism by using FE-SEM analysis results by the

study of effect of various reaction parameters. The inherent properties of the HNS-CeO_2 material are explored in detail with the assistance of various analytical and spectroscopic techniques in the above section. The observed inherent properties are highly recommended to verify the potential catalytic activity for CO_2 fixation reaction. The pyridine and chloroform analysis results evidently revealed that dual active sites (Lewis acidic and Lewis basic) are successfully engaged in the HNS-CeO_2 material. However, earlier reports are well recommended that dual active sites and reducing properties materials are highly suitable for the benzimidazole synthesis. So, initially using HNS-CeO_2 as a promising catalyst, we tested the benzimidazole reaction in the presence of model reagents of OPD and CO_2 under mild reaction conditions. Under catalyst-free reaction conditions at 100 °C for 12 h under 0.5 MPa pressure in the attendance of a base (K_2CO_3) and a reducing agent (DMAB), the benzimidazole reaction failed to achieve the desired product.[21, 22] The catalyst-free reaction results **(Table 1, entry 1)** illustrated the role of catalyst in getting the desired product with excellent yield and selectivity. Under similar reaction conditions, in the presence of HNS-CeO_2 catalyst the benzimidazole reaction successfully achieved 100% conversion of OPD and 96% yield and selectivity of the desired product **(Table 1, entry 2)**. Additionally, we tested the NS-$Ce(OH)_3$ as a catalyst for the benzimidazole reaction and found that achieved less yield of the desired product when compared to the HNS-CeO_2 catalyst **(Table 1, entry 3)**. However, formerly reported literature well advised that the base (K_2CO_3) and DMAB play a very intensive roles in the benzimidazole reaction.[22, 37] Evidently, we proved this by carrying out the benzimidazole reaction under base and DMAB-free conditions, and both reactions associatively achieved only 11% and 12% yields of the desired product **(Table 1, entries 4 and 5)**. So, from controlled experiments, it is evidently concluded that the benzimidazole reaction failed to achieve the desired product under base and DMAB-free conditions. Also, the tested Ce precursor ($(NH_4)_2$ Ce $(NO_3)_6$) and solvents (propanol and

glycerol) achieved very low yields of the benzimidazole product **(Table 1, entries 7-8)**. Additionally, we tested the morphology-free catalyst (CeO_2 powder) to prove to role of morphology in the benzimidazole formation process. The CeO_2 powder catalyst showed less yield of the desired product at 100 °C for 12 h **(Table 1, entry 9)**. Overall, the initial screening study results validated that the HNS-CeO_2 catalyst system could potentially have a great synergistic effect in the reaction medium. Hence, it was nominated as a highly selective and competent catalyst for the benzimidazole synthesis under mild, solvent-free reaction conditions and for further examinations.

Table 1: Initial Catalyst Screening Study for Benzimidazole Synthesis

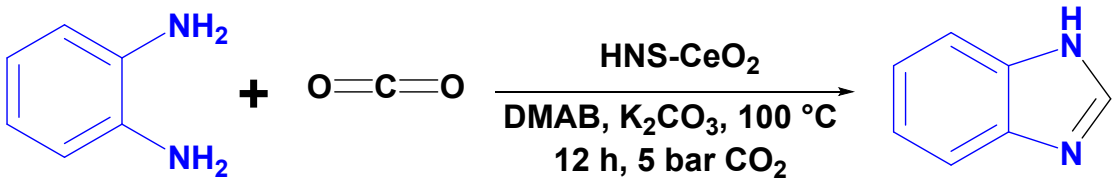

entry	catalyst	conversion (%)	selectivity (%)	yield (%)
1	catalyst free	40	15	6
2	**HNS-CeO_2**	**100**	**96**	**96**
3	NS-Ce $(OH)_3$	100	27	27
4	base free	100	11	11
5	DMAB free	58	0	0
6	$(NH_4)_2$ Ce $(NO_3)_6$	96	37	35
7	glycerol	75	11	8
8	propanol	80	22	18
9	CeO_2 powder	100	58	58

Typical reaction conditions: 1 mmol o-phenylenediamine (OPD) (100 mg), 5 wt. % catalyst with respect to OPD, 0.5 mmol base of K_2CO_3 (65 mg), 100 °C, 12 h, 0.5 MPa CO_2 pressure**,** 3 mmol of DMAB (165 mg), 800 rpm. Product was confirmed by GC, GC-MS, ^1H and ^{13}C NMR along with benzimidazole standard was used to confirm the desired product.

Using a promising HNS-CeO_2 catalyst, we examined different reaction variables for the synthesis of benzimidazole product. As we studied in the previous section, the base and DMAB reagents are play an intensive role in getting the desired product with high selectivity and yield. So, initially, we scrutinized the effects of base and DMAB amounts under mild reaction conditions of 5 wt.% catalyst amount, 100 °C for 12 h, and 0.5 MPa CO_2 pressure **(Figure 5 (a and b))**.

The positive effect on the benzimidazole yield and selectivity is clearly observed from the effect of base amount, as shown in **Figure 5 (a)**. When the cycloaddition reaction performed in the absence of base, it achieved only 11% yield and selectivity for the desired product. Further, by gradually upstairs the amount of base up to 0.4 mmol, the benzimidazole product failed to achieved >90% yield. So, when the cycloaddition reaction was carried out with a 0.5 mmol of base, it successfully attained the benzimidazole product with 100% conversion of OPD and 96% yield along with selectivity. After scrutinizing the benzimidazole reaction in higher-amount base conditions, there was no discernible improvement in the desired product yield and selectivity. So, the 0.5 mmol base amount is highly desirable to get the selective benzimidazole product.

Figure 5 (b) depicts the amount of DMAB that plays a very concentrated key role in the benzimidazole synthesis process over the HNS-CeO_2 catalyst. Previously, the tested DMAB-free reaction failed to detect the benzimidazole product under mild reaction conditions **(Table 1, entry 5)**. The influence of the DMAB amount was inspected in the range of 0 to 5 mmol. Under optimized reaction conditions, the lower DMAB amount reactions of 1 and 2 mmol concordantly achieved benzimidazole product yields of 32% and 72%, respectively. Later, the tested 3 mmol DMAB amount reaction showed 100% conversion of OPD and 96% yield, along with selectivity of the desired product. The catalyst-

free, DMAB-free, and lower DMAB amount reaction results are evidently showed that the conversion of OPD is completely reliant on DMAB and catalyst amount. The higher DMAB amount (4 and 5 mmol) reactions gradually observed less product yields. From the effect of base and DMAB study, 0.5 mmol of base and 3 mmol of DMAB reaction conditions are extremely suitable to achieve the highest yield of the desired product and selectively. Hence, same reaction conditions are elected as optimal reaction conditions for further various reaction parameter studies for the benzimidazole synthesis.

As shown in **Figure 5 (c)**, the active sites-free reaction achieved only a 10% yield of the benzimidazole. Further, we gradually increased the catalyst amount in the reaction medium up to 10 wt. % In the presence of 2.5 wt. % catalyst amount reaction achieved only 69% yield of the benzimidazole product due to the deficiency of active sites concentration in the reaction medium. However, a satisfactory number of active sites (5 wt. %) along with 0.5 mmol of base and 3 mmol of DMAB highly influenced to achieve more benzimidazole product yield (96%). Additionally, the tested higher catalyst amount reactions (7.5 wt. % and 10 wt. %) are observed a slight negative effect on the benzimidazole yields due to the presence of more active sites in the reaction medium.

As observed results from the effect of pressure study, the benzimidazole product yield and selectivity is highly reliant on it, as shown in **Figure 5 (d)**. Previously, few efficient catalysts were reported under atmospheric pressure in the presence of solvent medium. From the perspective of sustainability, initially we tested the benzimidazole reaction under atmospheric pressure under solvent-free reaction conditions. Also, we tested the benzimidazole reaction in the presence of ethanol as a polar solvent. But both solvent and solvent-free reactions are failed to attain the desired product at 5 wt.% catalyst dosage, 100 °C for 12 h. Further, under solvent-free reaction conditions, by increasing the reaction pressure by 2.5 bar due to the non-homogeneous phase in the reaction medium, the

benzimidazole product achieved only a 40% yield. Further, the tested 5 bar pressure reaction achieved a 96% yield of the benzimidazole due to the successful attainment of a homogeneous medium. The high-pressure reaction conditions are slightly observed less benzimidazole product yields due to the CO_2-rich phase in the reaction medium.

In the benzimidazole synthesis protocol, temperature plays a very attractive role in crossing the energy barrier in the reaction medium. The observed results are displayed in **Figure 5 (e)**. According to the observed results, the HNS-CeO_2 catalyst failed to achieve the complete conversion of OPD at RT due to the lower activation energy. Also, scrutinized higher reaction temperatures of 60 °C and 80 °C results evidently failed to improve the OPD conversion and the benzimidazole yield >90%. When the reaction was performed at 100 °C, the cycloaddition reaction successfully achieved 100% conversion of OPD and 96% yield of the benzimidazole product. Further, at elevated reaction temperatures of 120 °C and 140 °C, the desired product yields gradually decreased and reached 90% and 78%, respectively. Hence, it was determined that the 100 °C reaction temperature is highly suitable to carry out the cycloaddition reaction between OPD and CO_2 over the HNS-CeO_2 catalyst.

Figure 5 (f) represents the effect of time on the benzimidazole reaction. As shown in **Figure 5 (f)**, the benzimidazole product is highly dependent on the reaction time. Initially performed less time zone reactions of 4 h and 6 h showed less yield of the benzimidazole product with >96% conversion of OPD. Further, carried out the benzimidazole reaction for 8 h and 10 h at 100 °C with 5 bar pressure. But both the reactions failed to reach the desired product with high selectivity and yield. The tested 12 h reaction successfully achieved with the complete conversion of OPD and 96% selectivity, along with the yield of the desired product. Furthermore, we prolonged the reaction time for 16 h, but the benzimidazole product gradually decreased in the reaction medium. Finally, from the study of various reaction parameter effects, we concluded that the benzimidazole product was achieved with high

selectivity (96%) along with complete conversion (100%) of the initial reagent of OPD in the presence of 0.5 mmol base, 3 mmol DMAB, 5 wt.% catalyst amount, 5 bar pressure, and 100 °C for 12 h under solvent-free reaction conditions.

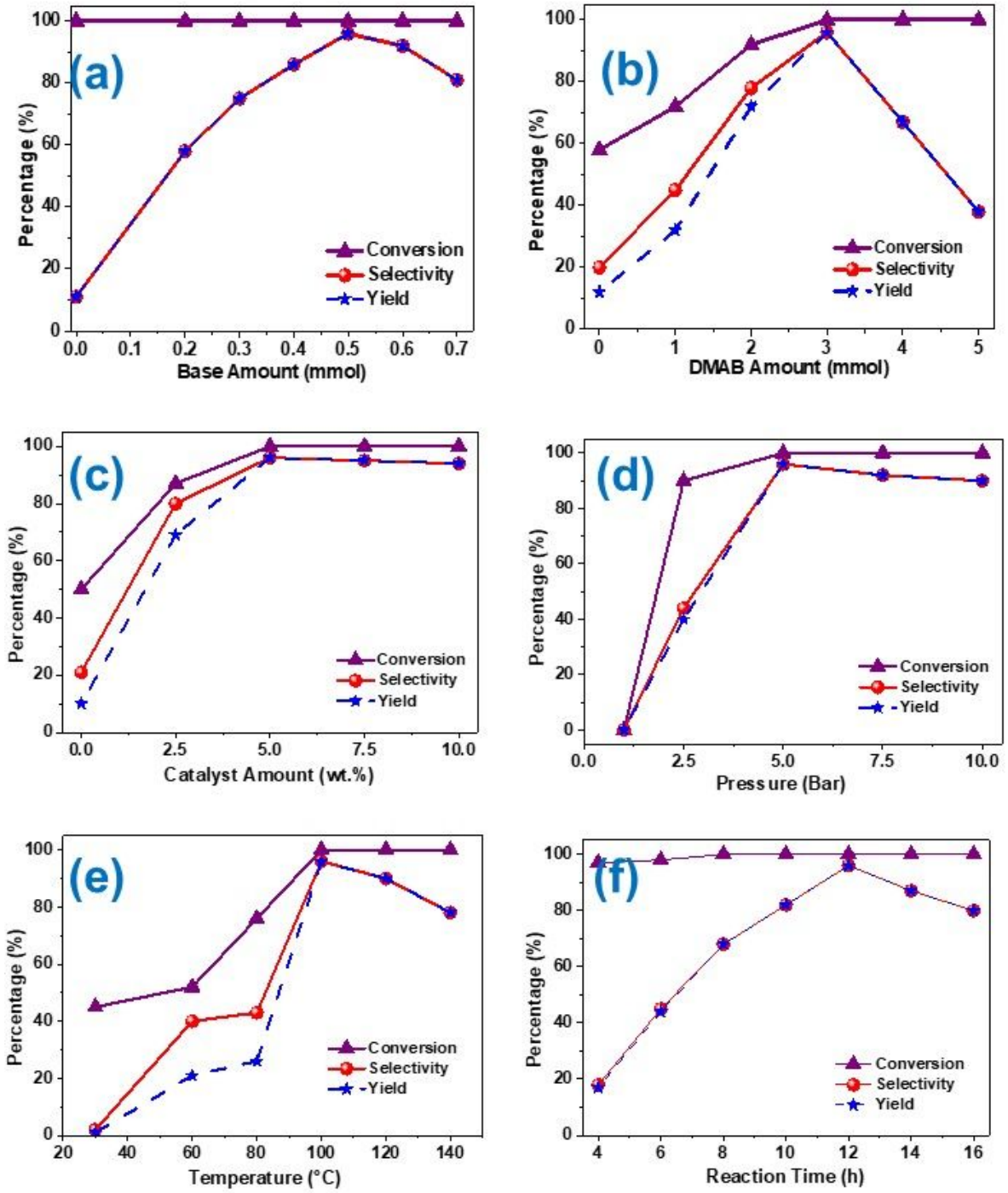

Figure 5. Effect of various reaction parameters **(a)** base, **(b)** DMAB, **(c)** catalyst dosage, **(d)** pressure, **(e)** temperature and **(f)** time.

From the initial catalyst screening study, we evidently confirmed that the HNS-CeO_2 catalyst is a highly selective and competent catalyst surface for the benzimidazole synthesis under temperate reaction conditions. Using the same catalytic surface, we examined various reaction parameters in detail for the benzimidazole reaction. Furthermore, we examine the XPS (X-ray photoelectron spectroscopy) analysis to probe the metallic state of the Ce and different kinds of oxygen species in the HNS-CeO_2 catalyst **(Figure 6)**. As shown in **Figure 6 (a)**, the full-scan survey spectrum clearly revealed the presented elements, namely cerium (Ce) and oxygen (O), in the HNS-CeO_2 catalyst without detecting any other impurity elements.[36] These results clearly indicated that the purity of the HNS-CeO_2 catalyst with the support of the XRD **(Figure 1 (b))** and EDAX analysis **(Figure S10 (a))** results.

The recorded specific Ce 3d core level spectra, after being deconvoluted (by Gaussian-Lorentzian function fitting), observed eight different binding energy peaks in the region of 875 to 925 eV, as shown in **Figure 6 (b)**. The core-level Ce 3d spectrum is divided into two important characteristic species, such as Ce^{+4} ($3d^{10}$ $4f^0$ state) and Ce^{+3} ($3d^{10}$ $4f^1$ state). The Ce^{+4} species observed Ce $3d_{5/2}$ and Ce $3d_{3/2}$ spin-orbit components. The observed different binding energy peak positions at 882.37 eV (v), 889.17 eV (v''), 898.48 eV (v''') and 900.86 eV (u), 907.48 eV (u''), 916.72 eV (u''') well correspond to the Ce $3d_{5/2}$ and Ce $3d_{3/2}$ spin-orbit components. The remaining binding energy peaks at 884.81 eV (v') and 903.07 eV (u') are assigned to the Ce^{+3} species. Cerium has excellent redox properties; hence, with the help of the Ce 3d spectrum, we estimated the Ce^{+3} concentration. The HNS-CeO_2 catalyst successfully observed the highest concentration of Ce^{+3} species (21.69%), which is completely proportional to the existence of Ce^{+3} defects and oxygen vacancies in the catalyst with a high concentration.[7, 8, 21]

The deconvoluted O 1s spectrum exhibits two successful different binding energy peaks situated at 529.44 eV and 531.51 eV, as displayed in **Figure 6 (c)**. These peaks are recommended as those of various kinds of oxygen species are occupied in the HNS-CeO_2 catalyst. The fitted peak at 529.44 eV is strongly attributed to lattice oxygens, which are generated by lattice O^{2-} species. Additionally, the shoulder peak at 531.51 eV is ascribed to the combination of surface oxygen species in the form of $O^{\delta-}$ and oxygen vacancies in the HNS-CeO_2 catalyst. The presence of lattice oxygen species is well coordinated with the Ce^{+4} species ($O-Ce^{4+}$). Similarly, observed surface oxygen species are generated with the help of the $O-Ce^{3+}$ bond. From these results evidently concluded that oxygen vacancies and Ce^{+3} species are successfully engaged in the synthesized catalyst. In order to get the amount of surface oxygen species, with the help of the O 1s spectrum, we found that 30% species are occupied in the HNS-CeO_2 catalyst.[35, 38] Finally, the C 1s spectrum was detected by the instrument itself **(Figure 6 (d))**.

XPS analysis results evidently indicates the presence of different Ce metallic states such as Ce^{4+} and Ce^{3+}, which are strongly suggested that they will act as a Lewis acidic site nature in the HNS-CeO_2 catalyst. Also, different oxygen species (surface oxygen and lattice oxygen) are strongly recommended as a Lewis basic site nature in the HNS-CeO_2 catalyst. Remarkably, different Ce (III) and Ce (IV) oxidation states, different oxygen species, and oxygen vacancies are highly favorable to enhance desired number of active sites (Lewis acidic and Lewis basic) in the promising HNS-CeO_2 catalyst. To support these results, the XRD, Raman, pyridine, and chloroform adsorption analysis results are well described in detail. Previously reported DFT (density functional theory) calculation results are well suggested that the achieved (111) plane of the HNS-CeO_2 catalyst will observe more stability when compared to other planes.[39] The Raman spectrum results revealed that the Ce-O bond and the presence of oxygen vacancies in the HNS-CeO_2 catalyst. Both pyridine and

chloroform adsorption analysis profiles detect Lewis acidic and Lewis basic site peaks at 1618 cm^{-1} and 2972 cm^{-1}, respectively. Considering both characteristic and experimental results, it is evident that both the Lewis acidic and Lewis basic site natures of the HNS-CeO_2 catalyst highly enhance the catalytic activity under temperate reaction conditions. Therefore, HNS-CeO_2 was selected as a highly promising and efficient catalyst surface for the selective synthesis of benzimidazole product.

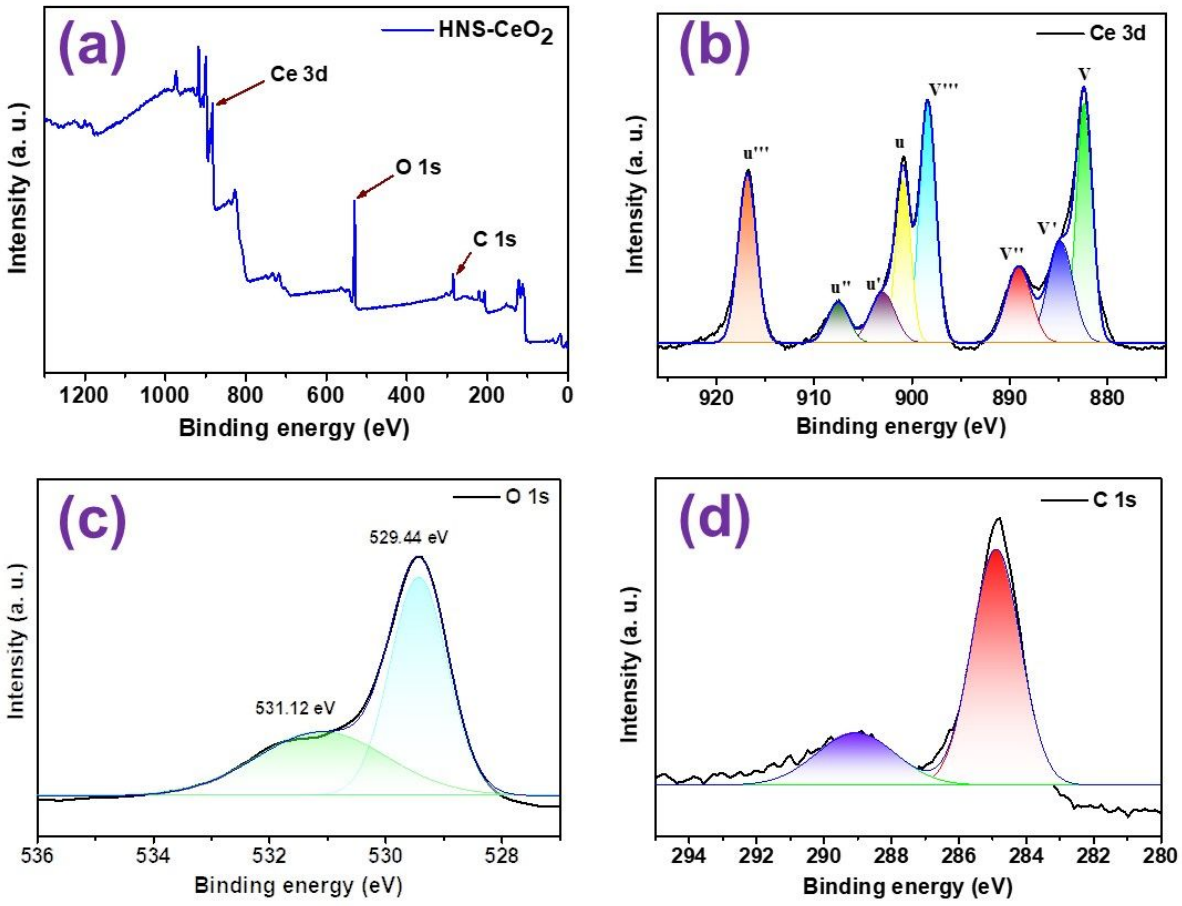

Figure 6. XPS analysis **(a)** Full scan survey spectrum, **(b)** Ce 3d, **(c)** O 1s and **(d)** C 1s spectra of the HNS-CeO_2 catalyst.

2.4 Chemical Fixation of CO_2 With Various Functional Groups Substituted Aromatic Diamines Over Efficient HNS-CeO_2 Catalyst

To exhibit the generality of HNS-CeO_2 as an efficient catalyst, different electron-donating and electron-withdrawing groups substituted o-phenylenediamine molecules were tested under optimized reaction conditions **(Table 2)**. As selected and all reactions were tested, the unsubstituted model reagent of o-phenylenediamine achieved excellent results, with a 96% yield and selectivity of the benzimidazole product at 100 °C for 12 h under pressurized reaction conditions (5 bar). The tested electron-donating groups such as CH_3 **(Table 2, entry 2)** and NO_2 **(Table 2, entry 3))** functionalized o-phenylenediamine substrates have shown negative influence in the reaction medium and achieved moderate yield of benzimidazole products under optimized reaction conditions. Whereas the halogen group (Cl) functionalized o-phenylenediamine molecule **(Table 2, entry 4)** allowed to interact with CO_2, it achieved only 52% conversion and 52% yield along with 100% selectivity of the desired product due to the electron withdrawing affinity in the reaction medium. Further, the HNS-CeO_2 catalyst showed good catalytic activity towards the bulky substrate of naphthalene-1, 8-diamine **(Table 2, entry 5)** and successfully achieved the desired benzimidazole product with 78% yield and 100% selectivity under optimized reaction conditions. Moreover, we synthesized the benzoxazole product under similar reaction conditions and achieved a moderate yield over an efficient HNS-CeO_2 catalyst **(Table 2, entry 6)**.[21, 22, 37] The obtained all results under optimized reaction conditions demonstrated that the HNS-CeO_2 is a promising and highly suitable catalyst to synthesis of various functional group-substituted benzimidazole products and different heterocyclic compounds.

Table 2. Substrate Scope Study Over HNS-CeO_2 Catalyst

Entry	Substrate	Product	Conversion (%)[a]	Selectivity (%)[a]	Yield (%)[a]
1	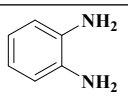	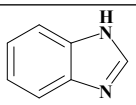	100	96	96

2	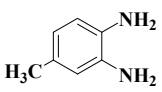	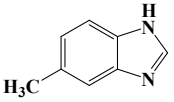	100	80	80
3	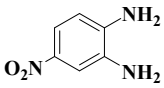	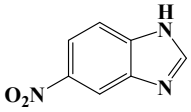	100	70	70
4	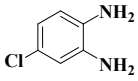	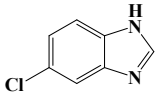	52	100	52
5	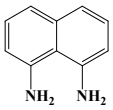	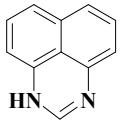	78	100	78
6		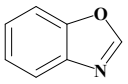	75	95	71

Optimized reaction conditions: 1 mmol substrate, 5 wt. % HNS-CeO_2 catalyst with respect to substrate (5 mg), 0.5 mmol base of K_2CO_3 (69 mg), 165 mg DMAB, 100 °C, 12 h, 5 bar CO_2 pressure, 800 rpm.

2.5 Hollow CeO_2 Nanospheres Catalyst Recyclability and Spent Catalyst Characterization Results

Recyclability is one of the most important criteria to evaluate promising heterogeneous catalysts feature from an industrial point of view.[40] After each cycloaddition reaction, the spent catalyst was collected by a simple centrifugation method and washed with ethyl acetate, ethanol, and distilled water. The obtained wet solid material dried at 150 °C overnight. Finally, the dried catalyst was tested for the benzimidazole synthesis using fresh reagents under optimized reaction conditions. As shown in **Figure 7**, the HNS-CeO_2 catalyst was successfully reusable for 15 consecutive cycles without declining its initial catalytic activity (96% yield and selectivity). To support the recyclability results, examined the leaching study and observed results are evidently represented the stable catalytic feature of the HNS-CeO_2 catalyst.[41] The HNS-CeO_2 catalyst was separated after 6 h from the reaction medium by a

simple centrifuge method and further allowed to run the reaction for a longer time zone (12 h) under optimized reaction conditions. **Figure S11** clearly displayed that the 6 h reaction achieved a 44% yield of the desired product. But, after filtration of the catalyst, the tested reaction up to 12 h achieved only 51% yield of the benzimidazole product. From these results, the HNS-CeO_2 catalyst was not leached out in the reaction medium. However, we observed less improvement (51%) in the product yield due to the presence of organic additives (base and DMAB) and reaction conditions.

Further, to support to the stable recyclability and leaching study results, we examined XRD, FE-SEM, EDAX, mapping, TEM/HR-TEM and XPS analysis to conclude crystallinity, surface morphology, presented elements, metallic state of the Ce and different kinds of oxygen species in the spent HNS-CeO_2 catalyst. **Figure S12 (a)** exhibits both fresh and spent catalyst XRD profiles, and the spent catalyst profile successfully regained its crystallinity after a number of recycles as well. The spent HNS-CeO_2 catalyst achieved hollow nanospheres morphology **(Figure S12 (b))**. Finally, without observing any derbies, the EDAX and mapping analysis results revealed that only detected Ce and O elements in the spent catalyst **(Figure S12 (c and d))**. From these results, we evidently concluded that the synthesized hollow nanospheres material is an efficient and reusable catalyst for benzimidazole synthesis. Additionally, we examined the XRD analysis for 5^{th}, 10^{th} and 15^{th} cycles spent catalysts. The attained XRD profiles of all spent catalysts well matched with the fresh HNS-CeO_2 catalyst profile as shown in **Figure S13**. Moreover, the TEM and HR-TEM analysis results evidently revealed the hollow nanospheres morphology of the spent catalyst **(Figure S14)**. The initial three images represent the TEM analysis results and these images clearly indicates the hollow nature by observing strong contrast between the intensely shady margins and the light pale region in the center **(Figure S14 (a-c))**. From HR-TEM analysis **(Figure S14 (d and e))**, calculated the lattice spacing value and obtained value of 0.248 nm is

well matched with the (220) plane of the spent catalyst **(Figure S14 (e))**. Also, in SAED pattern **(Figure S14 (f))** all concentric circles are well corresponds to the (hkl) values and it indicates the polycrystalline in nature. More evidently, scrutinized the XPS analysis for the spent catalyst to find metallic state of the Ce and different kind of oxygen species **(Figure S15)**. More evidently, the spent catalyst XPS analysis results revealed that the occupied Ce metallic states (Ce^{3+} and Ce^{4+}) and different kinds of oxygen species are successfully regained in the spent HNS-CeO_2 catalyst.

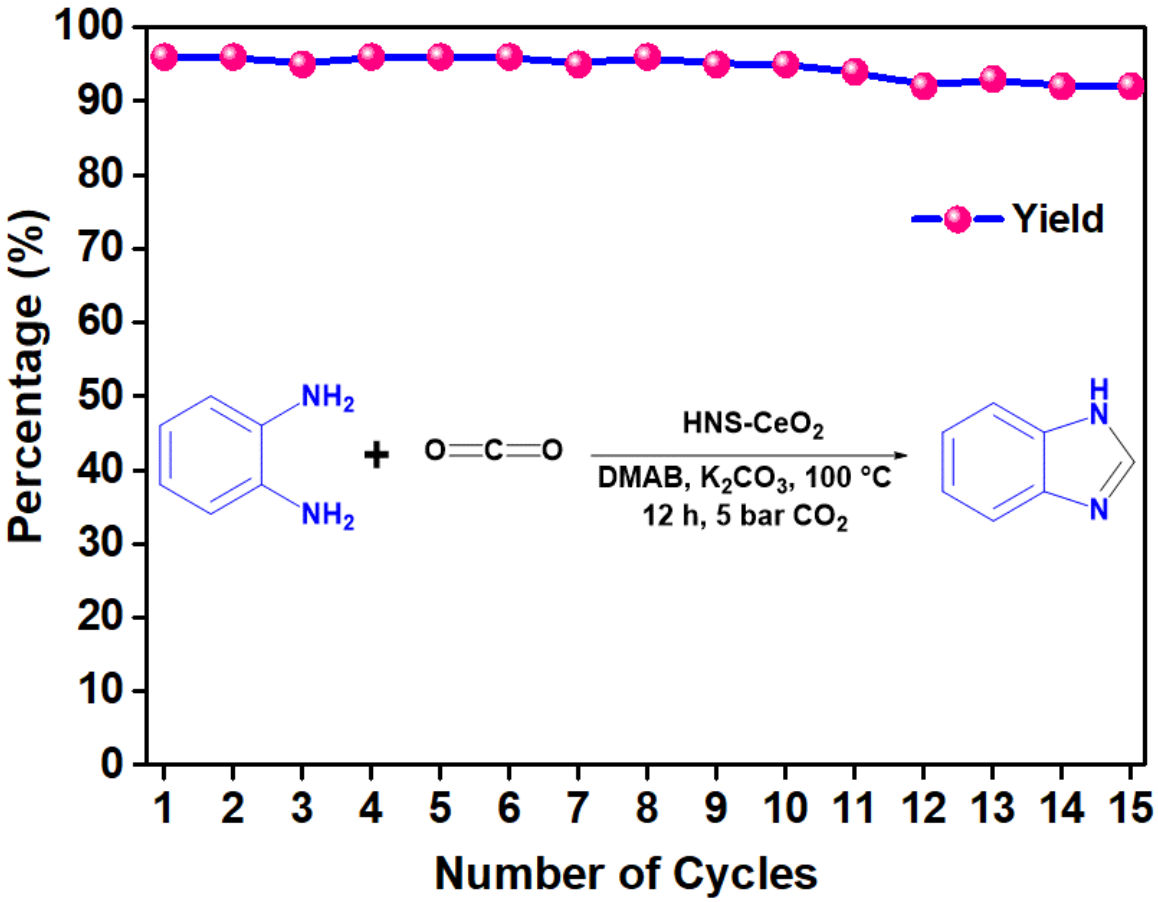

Figure 7. Recyclability test using HNS-CeO_2 catalyst. Reaction conditions: 1 mmol o-phenylenediamine (100 mg), 5 wt. % catalyst amount with respect to OPD (5 mg), 0.5 mmol base of K_2CO_3 (69 mg), 100 °C, 12 h, 5 bar CO_2 pressure, 165 mg DMAB (3 mmol), 800 rpm.

2.6 Evaluation of HNS-CeO_2 Catalytic Activity and Recyclability Results with Earlier Reported Catalysts

Successfully identified, HNS-CeO_2 has a highly potential catalyst surface for the benzimidazole synthesis under temperate reaction conditions in the absence of solvent medium. We deemed that the highly promising catalytic activity and recyclability results are noteworthy to compare with the formerly reported catalysts, as summarized in **Table S1**. At first, Liu et al. reported the $RuCl_2(dppe)_2$ catalyst for the benzimidazole synthesis via a cycloaddition reaction between OPD and CO_2 along with in the presence of H_2 medium **(Table S1, entry 1)**. The authors tested the $RuCl_2(dppe)_2$ catalyst under harsh reaction conditions and, most importantly, failed to recycled it for the CO_2 fixation reaction. The authors described the plausible reaction mechanism for the benzimidazole synthesis via the formic acid lane. After that, the reported homogeneous catalysts, namely, Ipr, CH_3COOK, $B(C_6F_5)_3$ and BBr_3 achieved excellent results under mild reaction conditions **(Table S1, entries 2-5)**. But reactions were carried out in phenylsilane and solvent medium to enhance the catalytic activity. Also, the homogeneous-featured catalysts are failed to show the recyclability feature for the cycloaddition reaction. Later, the reported polymer-supported zinc catalyst of PS-Zn (II)- SALTETA showed excellent catalytic activity under atmospheric pressure in the presence of solvent medium **(Table S1, entry 6)**. But the authors were failed to test the recyclability for the benzimidazole reaction. Next, reported both Ru@PsIL and Cu@U-g-C_3N_4 catalysts showed superior catalytic activity under high-pressure reaction conditions for a longer reaction time duration **(Table S1, entries 7 and 8)**. Both of the catalysts showed less than 5 recycles with less stable catalytic activity results under optimized reaction conditions. In 2020, Islam and co-workers reported the potential metalated COF catalyst (Cu-NPs@COF) for the benzimidazole synthesis under mild reaction conditions in the presence of EtOH: H_2O as a solvent medium and exhibited six consecutive recycles

with less stable catalytic activity **(Table S1, entry 9)**. Recently, our group reported the trimetallic scaffold catalyst for the benzimidazole reaction at high pressure reaction conditions and successfully recycled it for 12 cycles with stable catalytic activity **(Table S1, entry 10)**. In the present work, we designed the hollow CeO_2 nanospheres (HNS-CeO_2) catalyst via a simple and facile, eco-friendly solvothermal method under mild reaction conditions in the presence of green solvents, namely, glycerol and propanol. The designed material showed excellent inherent properties, such as hollow morphology and high thermal and structural stability. The observed inherent properties effectively enhanced the active site concentration and synergistic effect in the reaction medium. The HNS-CeO_2 catalyst showed superior catalytic activity under mild reaction conditions in the absence of polar and non-polar solvents. Also, the HNS-CeO_2 catalyst could be easily recovered by a simple filtration method and successfully recycled for 15 consecutive cycles with stable catalytic activity along with structural and physicochemical properties. Hence, we remarkably concluded that HNS-CeO_2 is a highly potential catalyst for the benzimidazole synthesis when compared to the formerly reported homogeneous and heterogeneous catalysts.

2.7 Plausible Reaction Mechanism for Benzimidazole Synthesis Over HNS-CeO_2 Catalyst

Scheme 1 represents the tentative reaction mechanism for the synthesis of benzimidazole in the attendance of HNS-CeO_2 catalyst surface. Previous reports have well recommended that the effective active sites of Lewis acidic and Lewis basic sites play a very intensive role in the benzimidazole synthesis process. Therefore, it is well described in detail about the effective active sites are successfully engaged in the HNS-CeO_2 catalyst with the help of various characterization techniques such as XRD, Raman, pyridine adsorption, chloroform adsorption, and XPS analysis. As synthesized, the HNS-CeO_2 catalyst evidently observed a

cubic-fluorite type phase with a (111) crystal phase. This crystal plane was successfully observed to have an intense Ce-O vibrational band unit in the catalyst. Also, the HNS-CeO_2 catalyst observed oxygen vacancies on its surface. Furthermore, the examined pyridine and chloroform analysis results evidently revealed the presence of Lewis acidic and uncoordinated oxygen sites in the HNS-CeO_2 catalyst. To support to these results, the XPS analysis results are more evidently revealed that Lewis acidic (Ce^{+4}, Ce^{+3}, and oxygen vacancies) and Lewis basic sites (lattice and surface oxygen species) are engaged in the synthesized HNS-CeO_2 catalyst.

The benzimidazole reaction mechanism will begin with the adsorption of CO_2 and DMAB reagents on the HNS-CeO_2 catalyst surface **(Step 1)**. After adsorption of both reagents **(Step 2)**, the highly stable CO_2 molecule was activated with the encouragement of Lewis basic sites. More interestingly, the observed oxygen vacancies in the HNS-CeO_2 catalyst also effectively activate the CO_2 molecule in the reaction medium.[36] Previous reports are well described; surface oxygen vacancy concentration directly enhances the CO_2 adsorption capacity on the catalyst surface. Oxygen vacancies permit them to interact with the non-bonding electron oxygen (O) atom of CO_2 via Lewis acidic and Lewis basic interactions. The interacted CO_2 molecule with oxygen vacancies produces bent (activated) CO_2^- intermediate species. Meanwhile, another molecule of DMAB is activated by the hydrogen bonding between the Lewis acidic site (B-H---Ce^{+4}/Ce^{+3}).[42] Subsequently, the activated CO_2^- species C-O bond intersection occurred with the B-H bond of the DMAB reagent **(Step 3)** and successfully produced the intermediate **C** species in **Step 3**.[43] After, the electron-rich reagent of OPD N atom interacted with the carbon of the activated CO_2 in the intermediate **C** to form a carbamate intermediate **D** species in **Step 4**. Further, the N- (2-aminophenyl) formamide intermediate was obtained by the elimination of hydroxy-N, N-dimethylamine borane in **Step 5**. Later, the N- (2-aminophenyl) formamide molecule in situ

intramolecular cyclization process was occurred with another electron-rich N atom of the OPD molecule **(Step 6)**. Next, the base will helps to abstract the proton (H) from the nitrogen atom to neutralize the N atom charge and to get the unstable benzimidazole molecule in **Step 7**.[21] Furthermore, by the dehydration process (-H_2O) and desorption of the catalyst surface successfully produced the stable cyclized benzimidazole product in the reaction mechanism **(Step 8)**.The eradicated catalyst surface is again engaged as an active surface in the reaction medium for the synthesis of the benzimidazole product.

In the benzimidazole synthesis process, effective active sites such as Lewis basic (lattice and surface oxygen species) and Lewis acidic (Ce^{+4}, Ce^{+3}, and oxygen vacancies) sites of the HNS-CeO_2 catalyst enhance the catalytic activity towards the desired product synthesis lane. More importantly, along with active sites, the presence of DMAB and base plays an intensive role in the benzimidazole formation process. Remarkably, with the aid of effective active sites, DMAB and base, we selectively synthesized the benzimidazole product with high yield under mild reaction conditions (100 °C, 12 h, 5 bar pressure, and solvent-free).

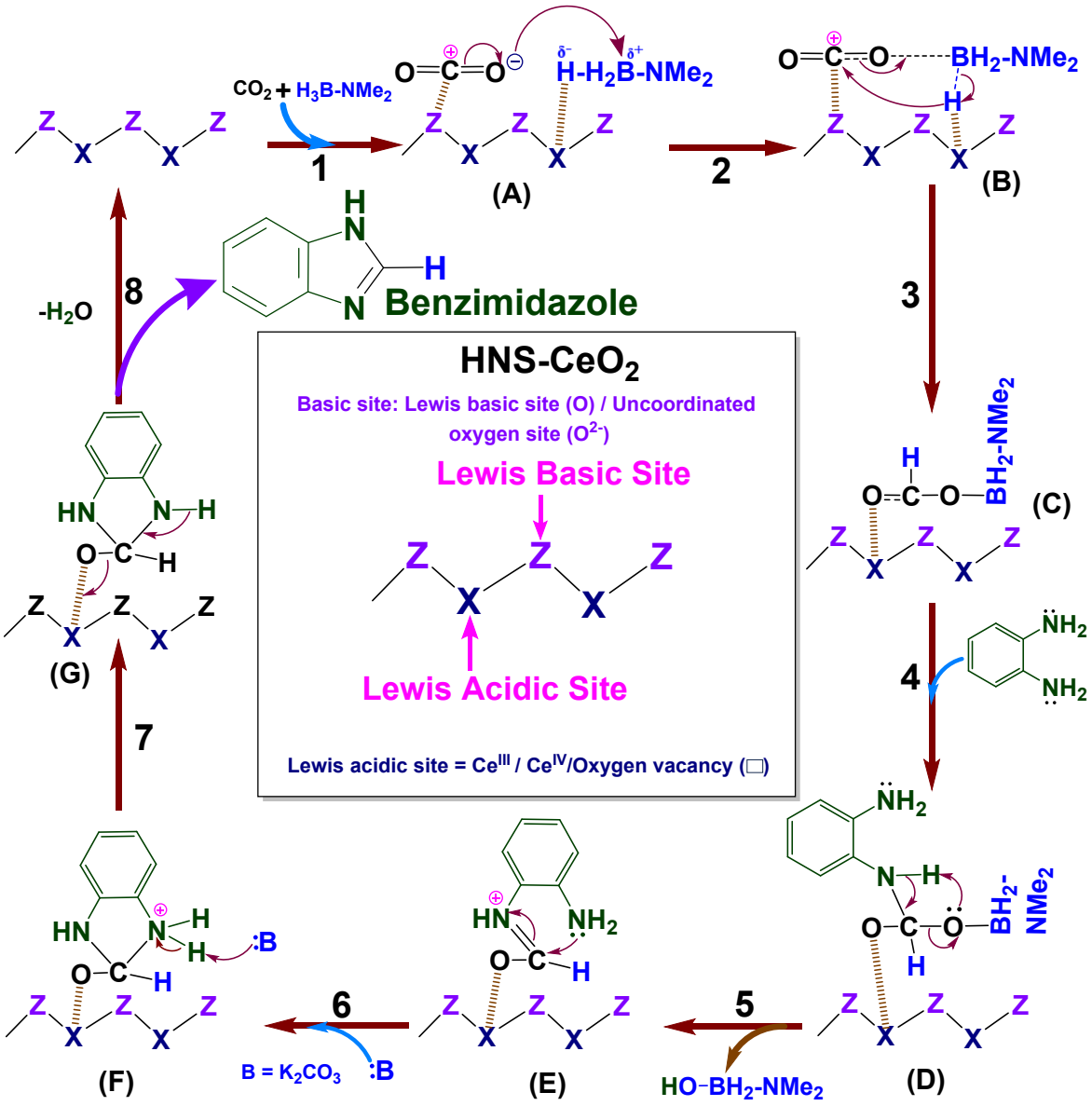

Scheme 1. Proposed the schematic representation for a plausible benzimidazole formation mechanism using HNS-CeO_2 catalyst.

3. CONCLUSION

In summary, utilized an efficient method of solvothermal and mild reaction conditions to design hollow CeO_2 nanospheres catalyst. Comprehensively examined effect of various reaction parameters to optimize hollow CeO_2 nanospheres morphology and successfully examined observed different surface architecture disparities using a FE-SEM analysis. The

HNS-CeO_2 material was well characterized to reveal its inherent properties by using various analytical and spectroscopic techniques. The efficient HNS-CeO_2 catalyst showed excellent catalytic activity (100% conversion and 96% selectivity and yield) for the CO_2 fixation reaction towards the benzimidazole product synthesis under mild and solvent-free reaction conditions using a model reagent of o-phenylenediamine. Optimized reaction conditions are effectively scrutinized by inspecting the effect of different reaction parameters such as effect of base amount, DMAB amount, catalyst dosage, temperature, pressure, and time. It was very interestingly revealed that the amount of base and DMAB plays a very intensive role to achieve the benzimidazole product with high selectivity under mild reaction conditions. Moreover, using HNS-CeO_2 catalyst synthesized different electron-donating and electron-withdrawing groups substituted benzimidazole compounds in moderate to excellent yields under optimized reaction conditions. With the support of characterization and experimental results, we proposed the tentative benzimidazole reaction mechanism and efficiently revealed the role and synergistic effect between Lewis acidic, Lewis basic, oxygen vacancies, DMAB, and base with model reagents of CO_2 and o-phenylenediamine. The tested competent catalyst of HNS-CeO_2 for the CO_2 fixation reaction remarkably showed excellent recyclability feature with stable catalytic activity, structural and physicochemical properties for up to fifteen consecutive cycles. The developed protocols for both catalyst synthesis and for CO_2 fixation reaction under mild reaction conditions gave great potential from the point of view of greener chemistry.

ACKNOWLEDGEMENTS

The authors would like to acknowledge the Science and Engineering Research Board (SERB), Government of India, for financial support through Core Research Grant (CRG) File no.- CRG/2021/000656.

AUTHORS INFORMATION

1. Puneethkumar M. Srinivasappa[a]- s.puneethkumar@jainuniversity.ac.in

   Address: [a]Centre for Nano and Material Science, JAIN University, Jain Global Campus, Bangalore 562112, Karnataka, India

2. Chob Singh[a]- chobs4295@gmail.com

   Address: [a]Centre for Nano and Material Science, JAIN University, Jain Global Campus, Bangalore 562112, Karnataka, India

3. Sarat Chandra Alla[a]- saratchandra444@gmail.com

   Address: [a]Centre for Nano and Material Science, JAIN University, Jain Global Campus, Bangalore 562112, Karnataka, India

4. Sandeep Suryabhan Gholap[b]- sandeep.gholap@isce2.a.star.edu.sg

   Address: Catalysis and Green Process Engineering, Institute of Sustainability for Chemicals, Energy and Environment, 1 Pesek Road, Jurong Island, Singapore 627833.

5. Akshaya K. Samal[a] - s.akshaya@jainuniversity.ac.in

   Address: [a]Centre for Nano and Material Science, JAIN University, Jain Global Campus, Bangalore 562112, Karnataka, India

6. Nitin K. Chaudhari[c]- nitin.chaudhari@sot.pdpu.ac.in

   Address: [c]Department of Chemistry, School of Technology, Pandit Deendayal Petroleum University, Gandhinagar, Gujarat, 382007, India

7. Arvind H. Jadhav*[,a] - j.arvind@jainuniversity.ac.in; jadhav.ah@gmail.com

   Address: [a]Centre for Nano and Material Science, JAIN University, Jain Global Campus, Bangalore 562112, Karnataka, India

NOTES

The authors declare no conflicts of interest.

REFERENCES

1. Yang, C.; Lu, Y.; Zhang, L.; Kong, Z.; Yang, T.; Tao, L.; Zou, Y.; Wang, S. J. S. S.Defect engineering on CeO_2-based catalysts for heterogeneous catalytic applications.Small Structures.**2021.***2*(12).2100058.
2. Montini, T.; Melchionna, M.; Monai, M.; Fornasiero, P. J. C. r.Fundamentals and catalytic applications of CeO_2-based materials.Chem. Rev.**2016.***116*(10).5987-6041.
3. Ziemba, M.; Schilling, C.; Ganduglia-Pirovano, M. V.; Hess, C. J. A. o. C. R.Toward an atomic-level understanding of ceria-based catalysts: when experiment and theory go hand in hand.Acc. Chem. Res.**2021.***54*(13).2884-2893.
4. Zhao, S.; Kang, D.; Liu, Y.; Wen, Y.; Xie, X.; Yi, H.; Tang, X. J. A. C.Spontaneous formation of asymmetric oxygen vacancies in transition-metal-doped CeO_2 nanorods with improved activity for carbonyl sulfide hydrolysis.ACS Catal.**2020.***10*(20).11739-11750.
5. Huang, X.; Zhang, K.; Peng, B.; Wang, G.; Muhler, M.; Wang, F. J. A. C.Ceria-based materials for thermocatalytic and photocatalytic organic synthesis.ACS Catal.**2021.***11*(15).9618-9678.
6. Miceli, P.; Bensaid, S.; Russo, N.; Fino, D. J. C. E. J.Effect of the morphological and surface properties of CeO_2-based catalysts on the soot oxidation activity.Chem. Eng. J.**2015.***278*190-198.
7. Feng, Z.; Ren, Q.; Peng, R.; Mo, S.; Zhang, M.; Fu, M.; Chen, L.; Ye, D. J. C. T.Effect of CeO_2 morphologies on toluene catalytic combustion.Catal. Today **2019.***332*177-182.

8. Yuan, S.; Zhang, Q.; Xu, B.; Jin, Z.; Zhang, Y.; Yang, Y.; Zhang, M.; Ohno, T. J. R. a.Porous cerium dioxide hollow spheres and their photocatalytic performance.RSC Adv.**2014.***4*(107).62255-62261.

9. Hu, J.; Deng, W.; Chen, D. J. A. S. C.; Engineering.Ceria hollow spheres as an adsorbent for efficient removal of acid dye.ACS Sustain. Chem. Eng.**2017.***5*(4).3570-3582.

10. GenericMesoporous CeO_2 hollow spheres prepared by Ostwald ripening and their environmental applicationsYang, Z.; Wei, J.; Yang, H.; Liu, L.; Liang, H.; Yang, Y., Mesoporous CeO_2 hollow spheres prepared by Ostwald ripening and their environmental applications. Chem., E. J. I., Ed. Wiley Online Library: 2010.

11. Wang, L.; Liu, F.; Yang, W.; Zhao, H.; Zheng, Y.; Chen, X.; Dong, W. J. M. L.Synthesis of multiple-shell porous CeO_2 hollow spheres by a hydrogel template method.Mater. Lett.**2013.***107*42-45.

12. Lai, X.; Halpert, J. E.; Wang, D. J. E.; Science, E.Recent advances in micro-/nano-structured hollow spheres for energy applications: From simple to complex systems.EES.**2012.***5*(2).5604-5618.

13. Raju, N. A.; Prasad, D.; Srinivasappa, P. M.; Biradar, A. V.; Gholap, S. S.; Samal, A. K.; Nagaraja, B. M.; Jadhav, A. H. J. S. E.; Fuels.Recent developments in state-of-the-art silica-modified catalysts for the fixation of CO_2 in epoxides to form organic carbonates.Sustainable Energy Fuels **2022.***6*(5).1198-1248.

14. Prasad, D.; Patil, K. N.; Chaudhari, N. K.; Kim, H.; Nagaraja, B. M.; Jadhav, A. H. J. C. R.Paving way for sustainable earth-abundant metal based catalysts for chemical fixation of CO_2 into epoxides for cyclic carbonate formation.Catal Rev Sci Eng.**2022.***64*(2).356-443.

15. Onyeaka, H.; Ekwebelem, O. J. I. J. o. E. S.; Technology.A review of recent advances in engineering bacteria for enhanced CO_2 capture and utilization.Int. J. Environ. Sci. Technol.**2023.***20*(4).4635-4648.
16. Srinivasappa, P. M.; Prasad, D.; Chaudhari, N. K.; Samal, A. K.; Thapa, R.; Siddharthan, E. E.; Jadhav, A. H. J. A. A. M.; Interfaces.Trimetallic Oxide Foam as an Efficient Catalyst for Fixation of CO_2 into Oxazolidinone: An Experimental and Theoretical Approach.ACS Appl. Mater. Interfaces **2023.***15*(18).21994-22011.
17. Mikkelsen, M.; Jørgensen, M.; Krebs, F. C. J. E.; Science, E.The teraton challenge. A review of fixation and transformation of carbon dioxide.EES **2010.***3*(1).43-81.
18. Tabanelli, T.; Bonincontro, D.; Albonetti, S.; Cavani, F., Conversion of CO_2 to valuable chemicals: organic carbonate as green candidates for the replacement of noxious reactants. In *Studies in Surface Science and Catalysis*, Elsevier: 2019; Vol. 178, pp 125-144.
19. Srinivasappa, P. M.; Bawiskar, D. B.; Manjunath, H.; Gholap, S. S.; Chaudhari, N. K.; Jadhav, A. H. J. E.; Fuels.Base-Tailored Hierarchical MgO Microspheres as Efficient Catalysts for CO_2 Fixation into Oxazolidinone at Atmospheric Pressure.Energy & Fuels **2023.***37*(18).14116-14130.
20. Vessally, E.; Didehban, K.; Babazadeh, M.; Hosseinian, A.; Edjlali, L. J. J. o. C. U.Chemical fixation of CO_2 with aniline derivatives: A new avenue to the synthesis of functionalized azole compounds (A review).J. CO_2 Util.**2017.***21*480-490.
21. Prasad, D.; Srinivasappa, P. M.; Raju, N. A.; Samal, A. K.; Jadhav, A. H. J. E.; Fuels.Stable Engineered Trimetallic Oxide Scaffold as a Catalyst for Enhanced Solvent-Free Conversion of CO_2 into Value-Added Products.Energy Fuels.**2023.***37*(2).1187-1206.

22. Khatun, R.; Biswas, S.; Biswas, I. H.; Riyajuddin, S.; Haque, N.; Ghosh, K.; Islam, S. M. J. J. o. C. U.Cu-NPs@ COF: A potential heterogeneous catalyst for CO_2 fixation to produce 2-oxazolidinones as well as benzimidazoles under moderate reaction conditions.J. CO_2 Util.**2020.***40*101180.
23. Kumar, P.; Kumar, A.; Joshi, C.; Singh, R.; Saran, S.; Jain, S. L. J. R. A.Heterostructured nanocomposite tin phthalocyanine@ mesoporous ceria (SnPc@ CeO_2) for photoreduction of CO_2 in visible light.RSC Adv.**2015.***5*(53).42414-42421.
24. Liang, Z.; Jiang, D.; Fang, G.; Leng, W.; Tu, P.; Tong, Y.; Liu, L.; Ni, J.; Li, X. J. C.Catalytic enhancement of aldol condensation by oxygen vacancy on CeO_2 catalysts.ChemistrySelect.**2019.***4*(14).4364-4370.
25. Prasad, D.; Patil, K. N.; Bhanushali, J. T.; Nagaraja, B. M.; Jadhav, A. H. J. C. S.; Technology.Sustainable fixation of CO_2 into epoxides to form cyclic carbonates using hollow marigold $CuCo_2O_4$ spinel microspheres as a robust catalyst.Catal. Sci. Technol.**2019.***9*(16).4393-4412.
26. Zhong, L.-S.; Hu, J.-S.; Cao, A.-M.; Liu, Q.; Song, W.-G.; Wan, L.-J. J. C. o. M.3D flowerlike ceria micro/nanocomposite structure and its application for water treatment and CO removal.Chem. Mater.**2007.***19*(7).1648-1655.
27. Wang, Z.; Hu, M.; Wang, Y.; Liu, X.; Qin, Y. J. J. o. A.; Compounds.Effect of solvothermal reaction temperature on the morphology of WO_3 nanocrystals and their low-temperature NO_2-sensing properties.J. Alloys Compd.**2016.***665*173-179.
28. Sun, C.; Li, H.; Zhang, H.; Wang, Z.; Chen, L. J. N.Controlled synthesis of CeO_2 nanorods by a solvothermal method.Nanotechnology.**2005.***16*(9).1454.
29. Zhang, D.; Du, X.; Shi, L.; Gao, R. J. D. t.Shape-controlled synthesis and catalytic application of ceria nanomaterials.Dalton Trans.**2012.***41*(48).14455-14475.

30. Wu, X.; Wei, M.; Yu, S.; Huang, J.; Sun, R.; Wong, C.-P. J. S. A. S.Formation of cerium oxide hollow spheres and investigation of hollowing mechanism.Appl. Sci.**2019.***1*1-9.

31. Wu, K.; Zhou, L.; Jia, C.-J.; Sun, L.-D.; Yan, C.-H. J. M. C. F.Pt-embedded-CeO_2 hollow spheres for enhancing CO oxidation performance.Mater. Chem. Front.**2017.***1*(9).1754-1763.

32. Li, D.; Qin, Q.; Duan, X.; Yang, J.; Guo, W.; Zheng, W. J. A. A. M.; Interfaces.General one-pot template-free hydrothermal method to metal oxide hollow spheres and their photocatalytic activities and lithium storage properties.ACS Appl. Mater. Interfaces.**2013.***5*(18).9095-9100.

33. Sonar, P.; Sanjeevagol, S.; Manjanna, J.; Patake, V.; Nitin, S. J. J. o. M. S. M. i. E.Electrochemical behavior of cerium (III) hydroxide thin-film electrode in aqueous and non-aqueous electrolyte for supercapacitor applications.J Mater Sci Mater Electron.**2022.***33*(34).25787-25795.

34. Dezfuli, A. S.; Ganjali, M. R.; Naderi, H. R.; Norouzi, P. J. R. A.A high performance supercapacitor based on a ceria/graphene nanocomposite synthesized by a facile sonochemical method.RSC Adv.**2015.***5*(57).46050-46058.

35. Liu, B.; Li, C.; Zhang, G.; Yao, X.; Chuang, S. S.; Li, Z. J. A. C.Oxygen vacancy promoting dimethyl carbonate synthesis from CO_2 and methanol over Zr-doped CeO_2 nanorods.ACS Catal.**2018.***8*(11).10446-10456.

36. Gong, Z.-J.; Li, Y.-R.; Wu, H.-L.; Lin, S. D.; Yu, W.-Y. J. A. C. B. E.Direct copolymerization of carbon dioxide and 1, 4-butanediol enhanced by ceria nanorod catalyst.Appl. Catal. B **2020.***265*118524.

37. Saptal, V. B.; Sasaki, T.; Bhanage, B. M. J. C.Ru@ PsIL-Catalyzed Synthesis of N-Formamides and Benzimidazole by using Carbon Dioxide and Dimethylamine Borane.ChemCatChem.**2018.***10*(12).2593-2600.

38. Kulal, N.; Vetrivel, R.; Ganesh Krishna, N.; Shanbhag, G. V. J. A. A. N. M.Zn-Doped CeO_2 nanorods for glycerol carbonylation with CO_2.ACS Appl. Nano Mater.**2021.***4*(5).4388-4397.

39. Werner, K.; Weng, X.; Calaza, F.; Sterrer, M.; Kropp, T.; Paier, J.; Sauer, J.; Wilde, M.; Fukutani, K.; Shaikhutdinov, S. J. J. o. t. A. C. S.Toward an understanding of selective alkyne hydrogenation on ceria: on the impact of O vacancies on H_2 interaction with CeO_2 (111).Am. Chem. J.**2017.***139*(48).17608-17616.

40. Bhanja, P.; Modak, A.; Bhaumik, A. J. C. A. E. J.Supported porous nanomaterials as efficient heterogeneous catalysts for CO_2 fixation reactions.Chem. Eur. J.**2018.***24*(29).7278-7297.

41. Kanakikodi, K. S.; Kulal, N.; Subramanya, K.; Puneethkumar, M.; Kulkarni, B. B.; Shanbhag, G. V.; Maradur, S. P. J. M. C.Effect of morphology and their oxygen vacancies of nanostructured CeO_2 catalyst for carboxymethylation of biomass-derived alcohols.Mol. Catal.**2024.***552*113667.

42. Biswas, I. H.; Biswas, S.; Islam, M. S.; Riyajuddin, S.; Sarkar, P.; Ghosh, K.; Islam, S. M. J. N. J. o. C.Catalytic synthesis of benzimidazoles and organic carbamates using a polymer supported zinc catalyst through CO_2 fixation.New J Chem.**2019.***43*(36).14643-14652.

43. Phatake, V. V.; Bhanage, B. M. J. C. L.Cu@UgC_3N_4 catalyzed cyclization of o-phenylenediamines for the synthesis of benzimidazoles by using CO_2 and dimethylamine borane as a hydrogen source.Catal Lett **2019.***149*347-359.